ACS APPLIED MATERIALS & INTERFACES

Research Article

www.acsami.org

Chlorhexidine-Loaded Amorphous Calcium Phosphate Nanoparticles for Inhibiting Degradation and Inducing Mineralization of Type I Collagen

Xue Cai,[†,∥] Bing Han,[†,∥] Yan Liu,[‡] Fucong Tian,[†] Fuxin Liang,[§] and Xiaoyan Wang*[,†]

[†]Department of Cariology and Endodontology, National Engineering Laboratory for Digital and Material Technology of Stomatology, Beijing Key Laboratory of Digital Stomatology, Peking University School and Hospital of Stomatology, Beijing 100081, P. R. China

[‡]Department of Orthodontics, National Engineering Laboratory for Digital and Material Technology of Stomatology, Beijing Key Laboratory of Digital Stomatology, Peking University School and Hospital of Stomatology, Beijing 100081, P. R. China

[§]State Key Laboratory of Polymer Physics and Chemistry, Institute of Chemistry, Chinese Academy of Sciences, Beijing 100190, P. R. China

ABSTRACT: A major shortcoming of contemporary dentin adhesives is their limited durability. Exposed collagen fibrils within the bonding interface are degraded by matrix metalloproteinases (MMPs), resulting in aging of the resin–dentin bond. In this study, chlorhexidine-loaded amorphous calcium phosphate (ACP) nanoparticles were synthesized to induce the mineralization of collagen fibrils. The nanoparticles sustainably released chlorhexidine to inhibit MMPs during mineralization. Three types of ACP nanoparticles were prepared: N-ACP containing no chlorhexidine, C-ACP containing chlorhexidine acetate, and G-ACP containing chlorhexidine gluconate, which had a higher drug-loading than C-ACP. Scanning and transmission electron microscopy indicated that the synthesized nanoparticles had diameters of less than 100 nm. Some had diameters of less than 40 nm, which was smaller than the width of gap zones in the collagen fibrils. Energy dispersive X-ray spectroscopy, Fourier-transform infrared spectroscopy, and high performance liquid chromatography confirmed the presence of chlorhexidine in the nanoparticles. X-ray diffraction confirmed that the nanoparticles were amorphous. The drug loading was 0.11% for C-ACP and 0.53% for G-ACP. In vitro release profiles indicated that chlorhexidine was released sustainably via first-order kinetics. Released chlorhexidine inhibited the degradation of collagen in human dentine powder, and its effect lasted longer than that of pure chlorhexidine of the same concentration. The ACP could induce the mineralization of self-assembled type I collagen fibrils. The chlorhexidine-loaded ACP nanoparticles sustainably released chlorhexidine and ACP under appropriate conditions. This is useful for inhibiting degradation and inducing the mineralization of dentine collagen fibrils.

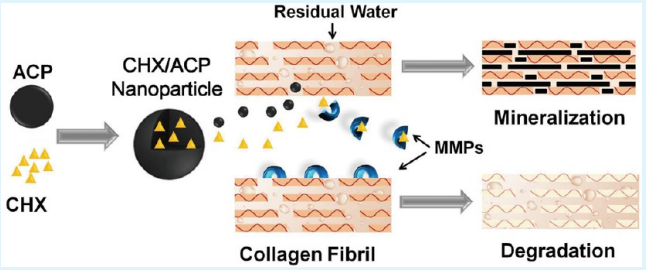

KEYWORDS: *amorphous calcium phosphate, chlorhexidine, sustained release, nanoparticle, mineralization, type I collagen*

1. INTRODUCTION

Biominerals such as bones and teeth are composites of an organic component, predominantly type I collagen, and an inorganic component, which is typically nanocrystalline with dimensions small enough to fit within the gap zones of type I collagen molecules.[1,2] The particular nanotopography of mineralized type I collagen fibrils affects the hardness and toughness of dentine,[3] and regulates the fate of certain cells within bone tissue.[4] Once biominerals begin to be demineralized, collagen fibrils become exposed to enzymes and are degraded, causing disintegration of the overall structure. The hardness and toughness of the biominerals are then significantly decreased.

Demineralization occurs in both pathological conditions such as dental caries and in intentional treatment procedures such as adhesive dentistry. Such bonding procedures use an etchant to expose collagen fibrils, as well as allow a monomer to infiltrate into the dentine to form resin tags. The resin monomer cannot completely displace water within the extrafibrillar and particularly the intrafibrillar compartments of the demineralized collagen matrix, so cannot completely infiltrate the collagen network.[5] This incomplete resin infiltration results in exposed unprotected collagen fibrils. The exposed fibrils are susceptible to creep[6] and cyclic fatigue rupture[7] after prolonged function. The acidic etchant can also activate the endogenous, bound matrix metalloproteinases (MMPs) and cysteine cathepsins,[3,8,9] which can also degrade collagen. This results in mineral-depleted, resin-sparse, water-rich regions along the bonding interface.[10−12] Under the combined challenges of enzyme, temperature, and functional stresses, the exposed collagen

Received: November 21, 2016
Accepted: February 23, 2017
Published: February 23, 2017

DOI: 10.1021/acsami.6b14956
ACS Appl. Mater. Interfaces 2017, 9, 12949−12958

fibrils within the dentin hybrid layer are susceptible to degradation, resulting in damage to the bonding interface and ultimately the failure of resin-dentin bonds.[13] Since adhesives are widely used in contemporary dentistry, their limited durability is a major problem. Replacing failed restorations in the United States of America is estimated to cost over five billion dollars per year.[14]

Several approaches have been investigated to improve bonding durability. These include increasing the degree of conversion and esterase resistance of hydrophilic adhesives, ethanol wet-bonding with hydrophobic resins, and exploiting collagenolytic enzyme inhibitors and cross-linking agents. The biomimetic remineralization of demineralized dentine matrix has also been investigated as a thorough method for strengthening the bonding interface.[13] However, the remineralization of dentine disks reportedly requires upward of four months.[3,15,16] Unprotected demineralized collagen fibrils may degrade during this period, causing loss of the remineralization template.

It is therefore important to both preserve the collagen template and shorten the remineralization time. MMPs are reportedly greatly involved in collagen degradation.[17] Chlorhexidine can inhibit MMPs by competitively chelating positive ions and then protecting the collagen template.[18] Studies indicate that 0.1−2% is an effective chlorhexidine concentration for achieving this.[5,19−21] However, electrostatically bound chlorhexidine can be competitively replaced by positive ions in dentinal tubules or dissolved by residual water within the extrafibrillar and intrafibrillar compartments of the collagen matrix.[22] This results in loss of the efficacy of chlorhexidine. Prolonged chlorhexidine delivery systems have been reported[23,24] but have involved polymer-based carriers which can cause toxicological problems upon degradation.[25] Developing better chlorhexidine sustained-release systems is therefore of interest.

The participation of amorphous calcium phosphate (ACP) in the early stages of the biomineralization of dentine has been demonstrated in vivo and is generally considered essential.[9,26] Collagen molecules self-assemble into fibrils with a specific tertiary structure, with a 67 nm periodicity, and 40 nm gaps between the ends of molecules.[27] These fibrils serve as a template for mineralization. The plasticity of liquid amorphous mineral precursors allows ACP to take the shape of its container, resulting in a variety of biominerals with different hierarchical structures.[28] ACP particles smaller than 40 nm initially infiltrate into the 40 nm gaps and then crystallize into apatite, which initiates intrafibrillar mineralization.[29] This is followed by interfibrillar mineralization to encapsulate the fibril.[9]

It occurred to us that chlorhexidine could be combined with ACP, as previous studies have used ACP as a drug carrier.[25,30,31] When ACP induces the mineralization of collagen fibrils, the sustained release of chlorhexidine could protect the collagen from degradation. ACP particles would act as a carrier and participate in mineral formation. Problems associated with polymer degradation would therefore be overcome. The release rates of Ca^{2+} and PO_4^{3-} from ACP nanoparticles are fast. This is because of the large surface area of ACP compared to that of other phases of calcium phosphate, such as dicalcium phosphate anhydrous (DCPA)[32] and could even be increased by lowering the pH.[33] Dentine tends to demineralize in acidic environments, so this characteristic of ACP could buffer the surrounding solution, as well as increase the calcium and phosphate contents.[33] It could also be useful for remineralization.

The current study aimed to synthesize chlorhexidine-loaded ACP nanoparticles and to explore their performance during the degradation and mineralization of collagen fibrils. The results provide a theoretical reference for dentine remineralization as well as enhancing bonding durability.

2. MATERIALS AND METHODS

Three types of ACP nanoparticles were prepared. N-ACP contained no chlorhexidine and was used as a negative control. C-ACP contained chlorhexidine acetate, and G-ACP contained chlorhexidine gluconate, which had a higher chlorhexidine loading than C-ACP.

2.1. Preparation of Chlorhexidine-Loaded ACP Nanoparticles. The template synthesis technique was used to prepare the three types of ACP nanoparticles (Figure 1). 0.15 g of PEG-6000 (Xilong, P. R. China) was dissolved in 3 mL of tris-HCl buffer solution (0.5 mol/L, pH 8, Xilong, P. R. China). For N-ACP, no further reagents were needed. For C-ACP and G-ACP, chlorhexidine acetate (Adamas, Switzerland) or chlorhexidine gluconate (Alfa Aesar, USA) was added to the solution to give a chlorhexidine concentration of 0.2 or 2%, respectively. 2.5 g of Tween 80 (Sigma-Aldrich, USA) was then added to form vesicles. The size of the vesicles was reduced by 40 kHz ultrasonic oscillation at 20−25 °C for 20 min (Biosonic UC100, Coltene Whaledent, USA). 3.55 mL of 0.175 mol/L calcium chloride (Xilong, P. R. China) solution was added, and the resulting solution was stirred for 30 min. 3.55 mL of 0.175 mol/L disodium hydrogen phosphate (Xilong, P. R. China) solution was then added. Seventeen microliters of poly(acrylic acid) (50 wt %, M_w 2 kDa, Sigma-Aldrich, USA) was then added to stabilize the newly formed ACP particles, and the resulting solution was stirred for 2 h. The ACP precipitate was then collected by centrifugation (5415R, Eppendorf, Germany), washed three times with deionized water, and lyophilized with a freeze-dryer (FD-1A-50, Boyikang, P. R. China).[34]

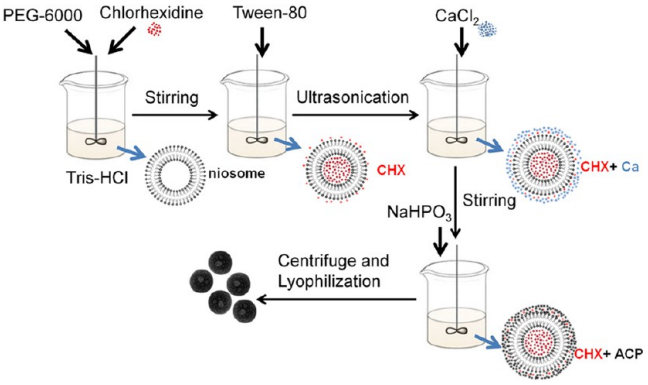

Figure 1. Schematic illustration of the preparation of the ACP nanoparticles.

2.2. Characterization of Chlorhexidine-Loaded ACP Nanoparticles. The surface morphology of the nanoparticles was observed using scanning electron microscopy (SEM) (S-4800, Hitachi, Japan). Chemical compositions were determined by energy dispersive X-ray spectroscopy (EDS) (S-4800, Hitachi, Japan). Samples were dispersed in ethanol, deposited on a silicon chip, allowed to dried, then sputter-coated with gold prior to observation.

The structures of the nanoparticles were observed using transmission electron microscopy (TEM) (JEM-1011, JEOL, Japan). Samples were dispersed in ethanol, deposited on carbon-coated copper grids, and allowed to dry prior to observation.

The surface area of the nanoparticles was estimated by the BET (Brunauer−Emmett−Teller) method, and the corresponding pore-volumes were calculated with the BJH method. Nitrogen adsorption/

DOI: 10.1021/acsami.6b14956
ACS Appl. Mater. Interfaces 2017, 9, 12949−12958

desorption isotherms were obtained (ASAP 2020, Micromeritics, USA).

The sizes of the ACP nanoparticles were determined by dynamic light scattering (DLS) measurements (Dynapro nanostar, Wyatt Technology, USA). The nanoparticles were suspended in deionized water, at a concentration of 0.1 mg/mL. Reported data are the average of triplicate measurements of samples prepared from three different preparations.

X-ray diffraction (XRD) (D/MAX 2500, Rigaku, Japan) was used to investigate the crystal structures of the ACP nanoparticles. Dried samples were loaded into a 20 × 15 × 2 mm slot in a glass slide and then analyzed. Cu K_α radiation (λ = 1.78897 Å) was used. Samples were scanned from 4−50°, with a step size of 0.02° and a scanning rate of 4°/min.

To determine the chlorhexidine loading (%), the entire nanoparticle sample (0.134 g) was dissolved in 5 mL of dilute hydrochloric acid. The solution was vigorously stirred, centrifuged, and the supernatant then analyzed by high performance liquid chromatography (HPLC) (1200, Agilent, USA). Analytical separation of chlorhexidine was carried out using a Zorbax Extend C-18 column (dimensions of 250 × 4.6 mm, internal diameter of 5 μm). The column temperature was maintained at 30 °C. The mobile phase was 0.01 mol/L disodium hydrogen phosphate solution (pH 2.5) and acetonitrile (65:35 V/V). The injection volume was 20 μL, the mobile phase flow rate was 1.0 mL/min, and the detection wavelength was 254 nm. Measurements were conducted in triplicate. The drug loading (%) of the microcapsules was calculated as drug loading (%) = weight of drug within nanoparticles/weight of nanoparticles × 100%.

2.3. In Vitro Release Profiles of Ca^{2+}, PO_4^{3-}, and Chlorhexidine. Fifty milligrams of nanoparticles were suspended in 1 mL of deionized water and then placed in a dialysis bag. The dialysis bag was kept in a serum bottle containing 50 mL of sodium chloride solution (0.133 g/mL) as the dissolution medium and was then buffered at three different pH conditions: pH 4 with lactic acid; pH 5.5 with acetic acid; and pH 7 with tris-HCl. Serum bottles were maintained at 25 °C and agitated at 50 rpm using a horizontal shaking incubator (WD-9405B, Liuyi, P. R. China). The pH of the dissolution medium was analyzed with a pH microelectrode (PHB-2, Sanxin, P. R. China) each day to ensure constant pH. Five samples were prepared for each type of nanoparticles at each pH. Thus, the total number of samples was 45 (five samples × three pH conditions × three nanoparticle types). At selected times, 200 μL aliquots were removed and replaced by an equal volume of fresh solution. The concentrations of Ca^{2+} and PO_4^{3-} in the removed aliquot were analyzed using an automatic Biochemical analyzer (7180, Hitachi, Japan), and its chlorhexidine concentration was analyzed by HPLC. The released ions and chlorhexidine are reported in cumulative concentrations.

2.4. Mineralization of Type I Collagen Fibrils with C-ACP and G-ACP. Self-assembled collagen fibrils were prepared as reported by Liu et al.[15] Specifically, a single layer of type I collagen fibrils was reconstituted over Formvar- and carbon-coated 400 mesh Ni TEM grids (Zhongjingkeyi, P. R. China), by neutralizing a 0.1 mg/mL collagen stock solution (pH 4−5) with 1 mol/L NaOH. To prepare the collagen stock solution, 100 μL of lyophilized type I collagen powder derived from rat tail (Corning, USA) was dissolved in 300 μL of acetic acid (0.1 mol/L, pH 3.0) and 400 μL of potassium solution which contained KCl (200 mmol/L), Na_2HPO_4 (30 mmol/L), and KH_2PO_4 (10 mmol/L). The neutralized collagen solution was left to gel by incubating at 37 °C for no more than 24 h. To stabilize the structure of the reconstituted collagen fibrils, collagen cross-linking was carried out using 0.3 mol/L 1-ethyl-3-(3-(dimethylamino)propyl)-carbodiimide (Sigma-Aldrich, USA) and 0.06 mol/L *N*-hydroxysuccinimide (Sigma-Aldrich, USA) for 4 h. Thereafter, collagen-coated grids were briefly immersed in deionized water and then dried in air. The mineralization of collagen fibrils was studied using four groups, whose conditions are described in Table 1.

The collagen-coated grids were placed upside-down over 100 μL droplets of liquid, inside a 100% humidity chamber for 72 h. The collagen-coated grids were then washed with deionized water, dried in air, observed by TEM, and analyzed by selected area electron diffraction (SAED).

Table 1. Experimental Conditions for the Four Groups Used in Collagen Fibril Mineralization Experiments

group	liquid drop
control	100 μL of deionized water
N-ACP	100 μL of deionized water contained 0.03g/mL N-ACP
C-ACP	100 μL of deionized water contained 0.03g/mL C-ACP
G-ACP	100 μL of deionized water contained 0.03g/mL G-ACP

2.5. Sustained Inhibition of Collagen Degradation by C-ACP and G-ACP. Twenty extracted sound human molars or premolars were obtained. The teeth were stored in 0.9% NaCl at 4 °C for less than three months. The coronal enamel and pulp tissue of each tooth was removed with a diamond bur under water-cooling. The remaining coronal dentine pieces were dried and ground into powder (particle diameter of 60−125 μm) with a GT200 grinder (Grinder, P. R. China), while frozen under liquid nitrogen.

Before experiments, the dentine powder was immersed in 100 μL of 35% phosphorous acid for 15 s and then washed twice with deionized water to activate the enzymes.[35] The six experimental groups each contained five samples. The six groups corresponded to the conditions given in Table 2.

Table 2. Experimental Conditions for the Six Groups Used in Collagen Degradation Inhibition Experiments[a]

group	dentine powder	deionized water	nanoparticles	chlorhexidine solution
control	20 mg	1 mL		
N-ACP	20 mg	1 mL	10 mg N-ACP	
0.11CHX	20 mg			0.11 wt %, 1 mL[b]
C-ACP	20 mg	1 mL	10 mg C-ACP	
0.53CHX	20 mg			0.53 wt %, 1 mL[b]
G-ACP	20 mg	1 mL	10 mg G-ACP	

[a]CHX indicates chlorhexidine. [b]According to the results, the drug loadings of the C-ACP and G-ACP nanoparticles were 0.11 and 0.53 wt %, respectively.

Samples were placed in a constant temperature and humidity chamber (LHS-250SC, Yiheng, P. R. China) at 37 °C. After 12, 24, 36, and 48 h, 300 μL aliquots were removed by centrifuging at 10 000 rpm and replaced with an equal volume of fresh solution to dilute the reaction solution. The concentrations of hydroxyproline (Hyp) were analyzed with an ELISA kit (TSZ, USA), to evaluate the degradation of collagen fibrils.

2.6. Statistical Analysis. Reported values were obtained as averages and are expressed as the mean ± standard deviation. Statistical analysis was performed by oneway ANOVA, using the SPSS 11.5 software package. For all tests, differences were considered statistically significant at α = 0.05.

3. RESULTS AND DISCUSSION

3.1. Synthesis and Characterization of Chlorhexidine-Loaded ACP Nanoparticles. Various techniques have been employed to synthesize ACP nanoparticles.[33] In the current study, PEG-6000 and Tween 80 formed stable niosomes at a certain ratio in aqueous solution. Ultrasonic oscillation reduced the size of the niosomes to the nanoscale.[36] The self-assembled niosomes could then encapsulate hydrophilic drugs, such as chlorohexidine, within their inner cavity.[37] When ACP formed nanoparticles based on the niosome template, chlorhexidine was encapsulated or adsorbed into the nanoparticles. The template was then removed in the washing process. This

DOI: 10.1021/acsami.6b14956
ACS Appl. Mater. Interfaces 2017, 9, 12949−12958

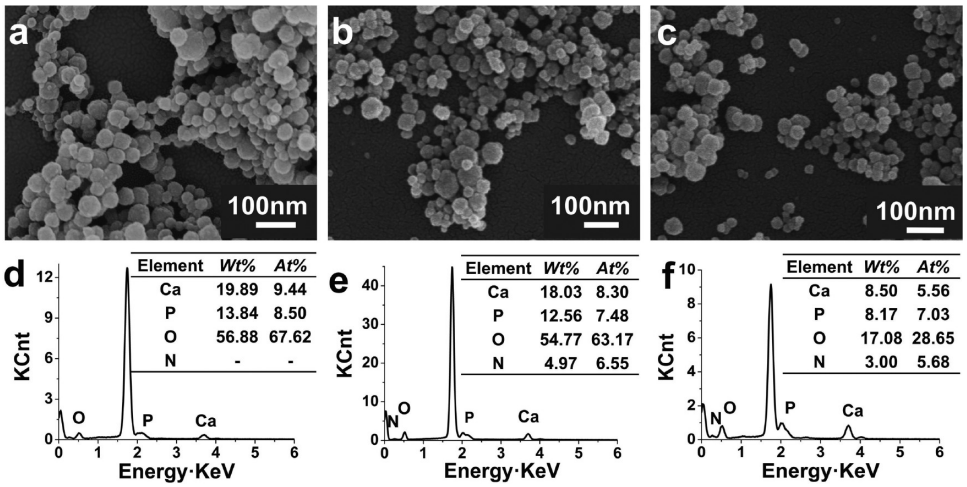

Figure 2. (a,b,c) SEM images of nanoparticles and their (d,e,f) EDS spectra: (a,d) N-ACP; (b,e) C-ACP; (c,f) G-ACP.

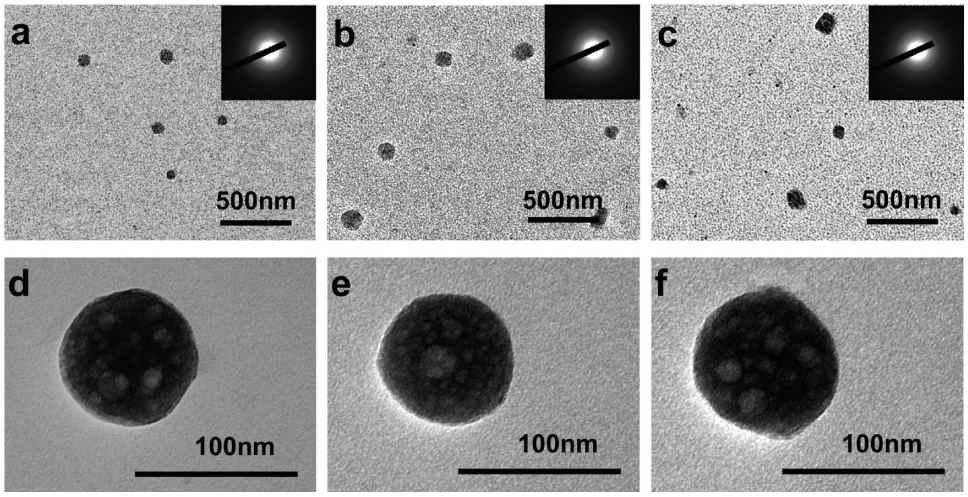

Figure 3. (a,b,c) Low magnification and (d,e,f) high magnification TEM images of nanoparticles: (a,d) N-ACP; (b,e) C-ACP; (c,f) G-ACP. The inset SAED figures show no diffraction patterns indicating the ACP is amorphous.

process was achieved under mild conditions, and no potential contaminants were introduced during template removal.

SEM images in Figure 2a–c show that the three types of nanoparticles all had uniform, spherical forms. The diameters of the final particles were <100 nm. Some particle diameters were also <40 nm, which was smaller than the width of gap zones in the collagen fibrils. As mentioned before, the mineral crystals initially deposited in the 40 nm-gaps of the collagen fibrils. This constituted intrafibrillar mineralization and was the initial and key process in collagen mineralization.[9] Thus, it is logical to assume that the ACP nanophases smaller than 40 nm are better, to penetrate and displace water from at least some internal compartments of the collagen fibrils.

EDS spectra in Figure 2d–f show that nitrogen signals were observed in the C-ACP and G-ACP nanoparticles but not in the N-ACP nanoparticles since the only nitrogen source was chlorhexidine. The two intense unlabeled peaks in Figure 2d–f were due to Si and Au, and resulted from the silicon chip and sputter-coated gold, respectively.

Representative TEM images in Figure 3a–c show the high dispersity of nanoparticles. Figure 3d–f show the synthesized nanoparticles contained numerous spherical surface protrusions. This suggested that particles were formed during the template synthesis process through the fusion of much smaller particles.[33] The inset SAED patterns indicate the ACP remains amorphous. An important feature of ACP is the porosity, which is highly desirable for drug or protein loading. The nitrogen adsorption/desorption method was employed to measure the BET surface area (Figure 4a–c). The BET surface area of the three representative nanoparticles is shown in Table 3. These unique characteristics lead to efficient diffusion of drugs in and out from the surface of the nanoparticles.[38] The BET surface areas of C-ACP and G-ACP were smaller than that of N-ACP. It may due to the adsorption of chlorhexidine in pores of C-ACP and G-ACP.

DLS measurements in Figures 4d show that the N-ACP, C-ACP, and G-ACP nanoparticles had average sizes of 86.4 ± 2.1, 87.1 ± 4.1, and 87.6 ± 4.6 nm, respectively. No statistical difference was found among 3 types of nanoparticles.

The XRD patterns in Figure 5a show a broad diffraction halo at 20–40° 2θ for the three types of ACP nanoparticles, suggesting that they were all amorphous. Pure ACP is highly unstable and can be stabilized by acidic noncollagenous proteins or magnesium ions.[39] Polyacrylic acid (PAA) possesses abundant carboxylate groups, which render it highly anionic and acidic. This enables PAA to inhibit mineral crystallization

DOI: 10.1021/acsami.6b14956
ACS Appl. Mater. Interfaces 2017, 9, 12949–12958

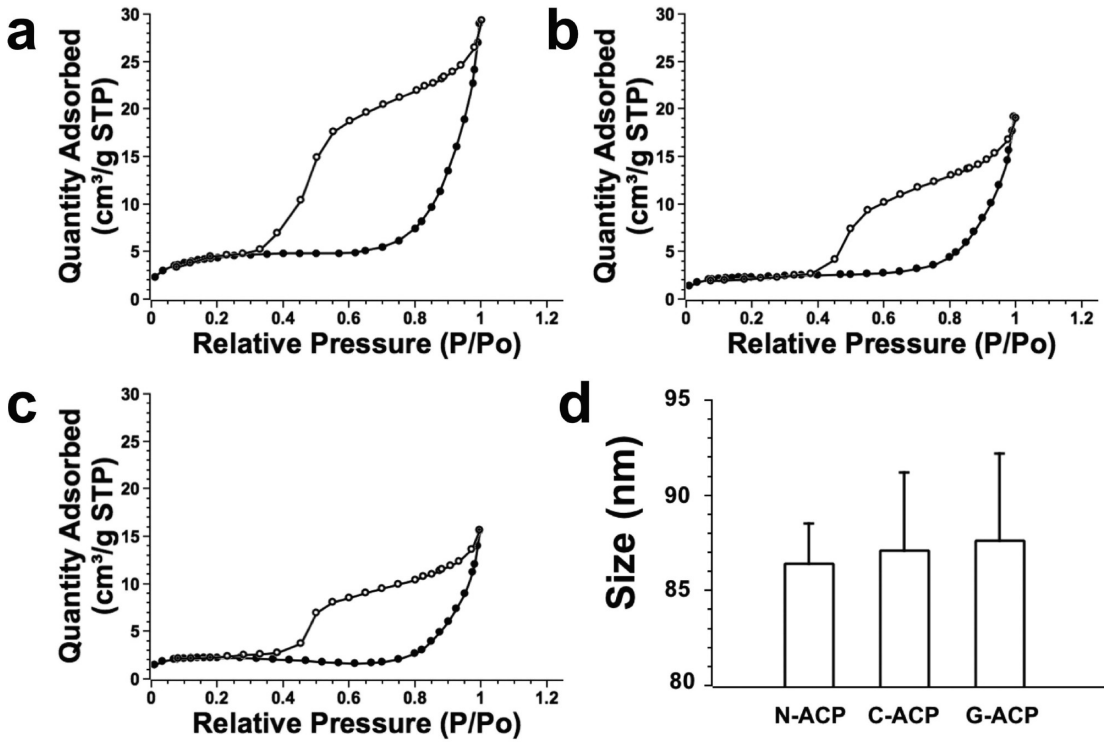

Figure 4. Nitrogen adsorption/desorption isotherms of representative nanoparticles: (a) N-ACP; (b) C-ACP; (c) G-ACP. (d) Diameters of different nanoparticles.

Table 3. BET Surface Area and Single-Point Total Pore Volume of the Three Representative Nanoparticles

group	surface area (m^2/g)	pore volume (cm^3/g)
N-ACP	14.51	0.04
C-ACP	7.28	0.03
G-ACP	6.14	0.02

and maintain nanoscale ACP in solution.[40] Without PAA, only large ACP nanoparticle aggregates could be identified along collagen fibril surfaces,[15] and intrafibrillar mineralization could not be achieved. Wang et al. reported that dentin could be remineralized in a biomimetic progression in the presence of 500 μg/mL PAA.[3] The resulting dentin had comparable structural features to those of natural dentin. The current study also used 500 μg/mL PAA to stabilize ACP, and similar results were observed.

Fourier-transform infrared (FTIR) spectra in Figure 5b show the functional groups that were present in the nanoparticles. The intense peaks at 1083 and 580 cm^{-1} were assigned to PO_4^{3-} as pointed out with the red arrow. The presence of these two peaks also supports the conclusion that the nanoparticles were amorphous. The transformation of ACP to hydroxyapatite (HA) is reportedly differentiated by the gradual splitting of the single peak at 580 cm^{-1} into two peaks at 600 and 560 cm^{-1}.[3] A mild peak at 950 cm^{-1} was also assigned to PO_4^{3-} as pointed

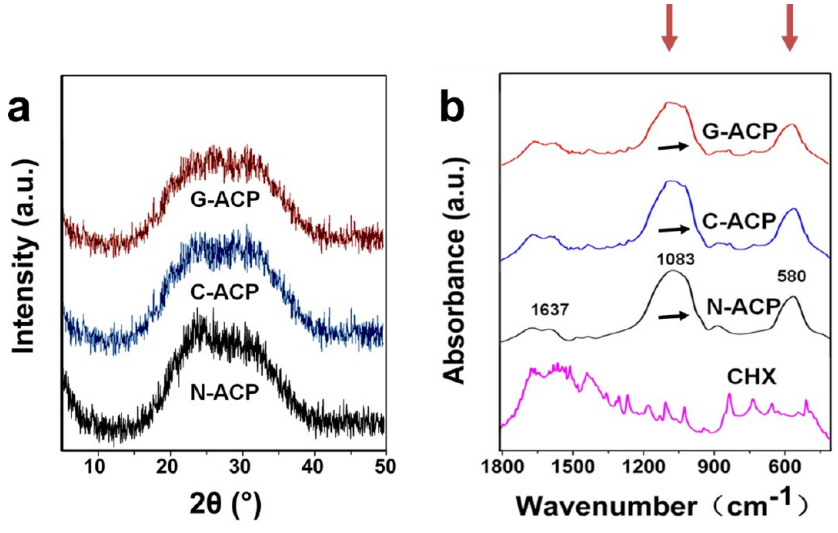

Figure 5. (a) XRD patterns of N-ACP, C-ACP, and G-ACP. (b) FTIR spectra of chlorhexidine (CHX), N-ACP, C-ACP, and G-ACP.

DOI: 10.1021/acsami.6b14956
ACS Appl. Mater. Interfaces 2017, 9, 12949−12958

out with a black arrow.[30] The peak at 1637 cm^{-1} was assigned to the O−H bending vibration. Peaks in the range 1600−1100 cm^{-1} were assigned to the C═N and C−N−C stretching vibrations, which are characteristic of chlorhexidine. Their presence suggested that chlorhexidine was present in the nanoparticles and had not reacted with ACP. Some of these peaks overlapped with that of PO_4^{3-}.

Mean drug loadings (%), standard deviations, and encapsulation efficiencies (%) of C-ACP and G-ACP are listed in Table 4.

Table 4. Drug Loadings and Encapsulation Efficiencies of C-ACP and G-ACP Nanoparticles

sample	drug loading (%)	encapsulation efficiency (%)
C-ACP	0.11 ± 0.01	0.49 ± 0.05
G-ACP	0.53 ± 0.04	0.24 ± 0.02

3.2. In Vitro Release Profiles of Ca^{2+}, PO_4^{3-}, and Chlorhexidine. The release profiles in Figure 6 show that loaded chlorhexidine was initially released rapidly from the C-ACP and G-ACP nanoparticles and that the release slowed after 1 day, becoming much more sustained. No statistical differences were observed in the chlorhexidine release for the three pH groups of the C-ACP and G-ACP nanoparticles.

Three commonly used drug release kinetics equations indicated that the C-ACP and G-ACP nanoparticles released chlorhexidine largely via first-order kinetics, as shown in Table 5.

Pharmaceutical dosage forms that obey first-order kinetics, such as water-soluble drugs in porous matrices, release drugs in a way that is proportional to the amount of drug remaining in their interior. Thus, the amount of drug released per unit time diminishes over time.[41] As the chlorhexidine is a kind of water-soluble drug which is encapsulated in the hydrophilic cavity of niosomes, it would be in the central part of the nanoparticles. Its slower release may have resulted from the barrier effect of the ACP matrix. However, the ACP matrix is porous. That made diffusion an important release mechanism as well.[41] This plus the high osmotic pressure in the early stage might cause both C-ACP and G-ACP showed the burst of release during the first 24 h. This burst of release would quickly increase the concentration of chlorhexidine to an effective concentration, which may be beneficial for controlling MMP activity in the early stages of using dentine and explain the pH independent release of chlorhexidine.

The in vitro release of calcium and phosphate ions is presented in Figure 7. An initial burst of Ca^{2+} and PO_4^{3-} release was observed in the first 3 days, which then slowed to a steadier release. Decreasing the pH from 7.0 to 4.0 resulted in a 1.2−1.7 times faster release of Ca^{2+} and PO_4^{3-}. In oral cavities, a local plaque pH of >6.0 is considered the safe zone, pH 6.0−5.5 is potentially cariogenic, and pH 5.5−4.0 is the cariogenic or danger zone leading to demineralization.[42] The demineralization or remineralization process in teeth depends on the pH and ion saturation of the surrounding solution. So the current trend in Ca^{2+} and PO_4^{3-} release buffered the surrounding solution and increased the ion saturation, which are beneficial for remineralization.

3.3. Mineralization of Type I Collagen Fibrils with C-ACP and G-ACP. Purified rat tail type I collagen can self-assemble into fibrils in slightly acidic environments. It is a single-layer hierarchical activated template and an appropriate mineralization model.[15] This model involves no noncollagenous proteins, so can be used to evaluate the mineralization effect of C-ACP and G-ACP.[9] As shown in Figure 8a, after reaction with distilled water for 72 h, collagen fibrils in the control group exhibited smooth edges and specific 67 nm periodic stripes, which consisted of gaps and overlap zones. This confirmed that reconstituted type I collagen fibrils did not induce mineralization alone.

Collagen fibrils exposed to N-ACP exhibited higher contrast and rough edges, as shown in Figure 8b. The stripes could no longer be observed by TEM. The SAED image of the intrafibrillar nanocrystals shown in the inset in Figure 8b indicated distinct arc-shaped patterns characteristic of hydroxyapatite. The orientation of the hydroxyapatite (002) reflection was parallel to the collagen reflection. This indicated that the crystalline c axes and axial direction of the mineralized fibril were aligned. Collagen fibrils exposed to C-ACP and G-ACP showed similar results to that exposed to N-ACP, as shown in Figure 8c and d, respectively. This indicated that the C-ACP and G-ACP nanoparticles could replace water in the intrafibrillar compartments and mineralize the collagen fibrils. The loading of chlorhexidine would not influence the mineralization procedure. This is significant for the remineralization of collagen fibrils in dentine hybrid layers.

Elemental maps of identical mineralized collagen fibrils indicated the spatial distribution of Ca and C. As shown in Figure 9, the signals of Ca and C were overlapped and uniformly distributed. This indicated that apatite had deposited uniformly throughout the entire collagen fibril.

Various types of biominerals are created by the different hierarchical structures of templates. In organic−inorganic nanometer-scale compound tissue, such as bone and teeth, self-assembled collagen proteins provide a template for the nucleation and multiplication of minerals. Noncollagenous proteins reportedly stabilize ACP precursors and direct the

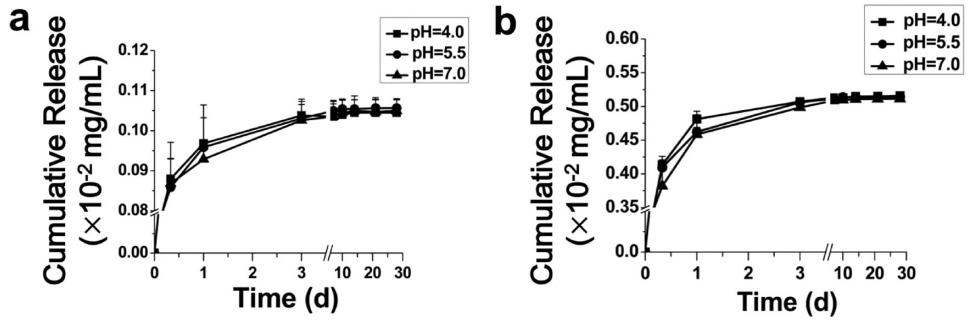

Figure 6. In vitro release profiles of chlorhexidine by (a) C-ACP and (b) G-ACP nanoparticles.

DOI: 10.1021/acsami.6b14956
ACS Appl. Mater. Interfaces 2017, 9, 12949−12958

Table 5. Chlorhexidine Release Kinetics of the C-ACP and G-ACP Nanoparticles[a]

samples		zero order kinetics	first order kinetics	Higuchi model
C-ACP	pH = 4.0	$Q = 0.003t + 0.727$	$\mathrm{Ln}\,(1 - Q) = -0.023t + 1.274$	$Q = 0.037t^{1/2} + 0.656$
		$R^2 = 0.755$	$R^2 = 0.919$	$R^2 = 0.889$
	pH = 5.5	$Q = 0.003t + 0.716$	$\mathrm{Ln}\,(1 - Q) = -0.022t + 1.232$	$Q = 0.037t^{1/2} + 0.644$
		$R^2 = 0.781$	$R^2 = 0.925$	$R^2 = 0.909$
	pH = 7.0	$Q = 0.003t + 0.711$	$\mathrm{Ln}\,(1 - Q) = -0.021t + 1.205$	$Q = 0.036t^{1/2} + 0.642$
		$R^2 = 0.804$	$R^2 = 0.947$	$R^2 = 0.915$
G-ACP	pH = 4.0	$Q = 0.006t + 0.572$	$\mathrm{Ln}\,(1 - Q) = -0.034t + 0.907$	$Q = 0.074t^{1/2} + 0.420$
		$R^2 = 0.525$	$R^2 = 0.808$	$R^2 = 0.691$
	pH = 5.5	$Q = 0.006t + 0.553$	$\mathrm{Ln}\,(1 - Q) = -0.033t + 0.822$	$Q = 0.075t^{1/2} + 0.401$
		$R^2 = 0.551$	$R^2 = 0.863$	$R^2 = 0.710$
	pH = 7.0	$Q = 0.006t + 0.523$	$\mathrm{Ln}\,(1 - Q) = -0.031t + 0.754$	$Q = 0.077t^{1/2} + 0.368$
		$R^2 = 0.598$	$R^2 = 0.854$	$R^2 = 0.759$

[a]Note: Q is the cumulative release rate at time t.

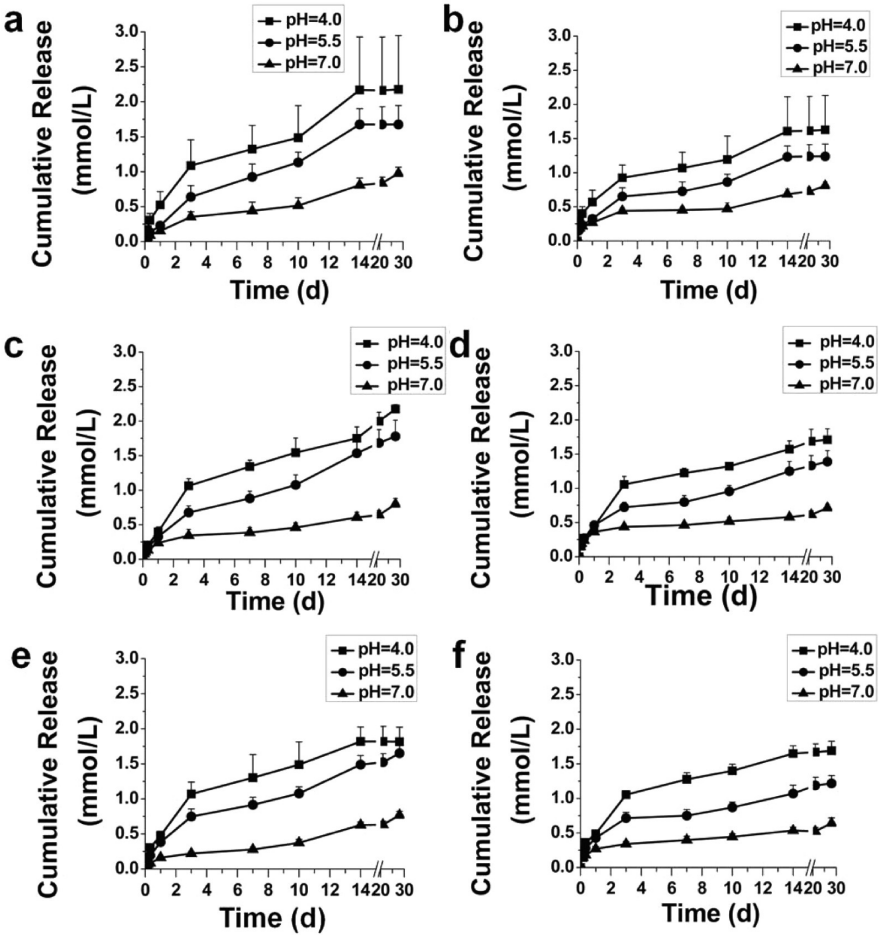

Figure 7. In vitro release profiles of Ca^{2+} from (a) N-ACP, (c) C-ACP, and (e) G-ACP nanoparticles, and PO_4^{3-} from (b) N-ACP, (d) C-ACP, and (f) G-ACP nanoparticles.

crystallization of biominerals.[16] A sequestration biomimetic analogue is required to simulate the function of these natural protein molecules. Dentin matrix protein-1 (DMP-1) is an acidic matrix protein, which can be cleaved into larger N-terminal and smaller C-terminal fragments. The aspartic acid rich N-terminal segment can help stabilize ACP nanoparticles.[43] In the current study, PAA was used to simulate the N-terminal segment of DMP-1, as the abundant carboxylate groups rendered PAA highly anionic and acidic. The resulting PAA-stabilized ACP nanoparticles were stable and could diffuse into the 40 nm gap zones.[15]

3.4. Inhibition of Collagen Degradation by C-ACP and G-ACP. Dentine collagen fibrils are degraded into polypeptides and then amino acids, upon exposure to MMPs. In this experiment, the dentine was ground to powder to provide larger contact area and shorter reactive time. It is a simplified model of real dentine disk. The liquid nitrogen can avoid the inactivation of MMPs when grinding. 35% phosphorous acid was used to simulate the etching procedure in dental clinic to

DOI: 10.1021/acsami.6b14956
ACS Appl. Mater. Interfaces 2017, 9, 12949−12958

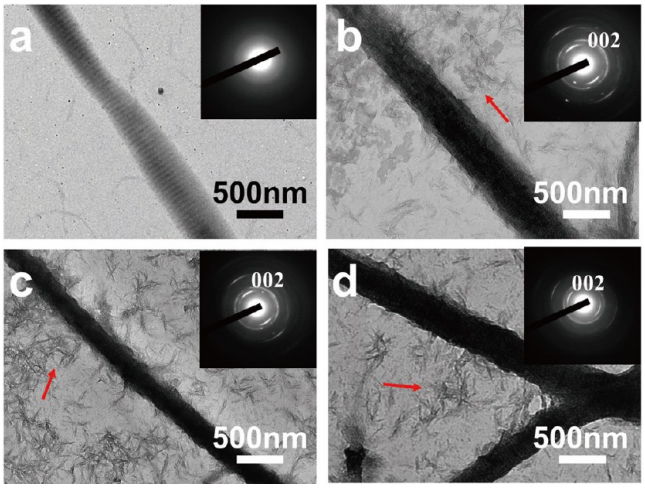

Figure 8. TEM images of unstained collagen fibrils after exposure to (a) deionized water, (b) N-ACP, (c) C-ACP, and (d) G-ACP. Obvious banding patterns are observed in the unmineralized nanofibers in panel a. SAED patterns (inset) of the intrafibrillar nanocrystals show distinct arc-shaped patterns characteristic of hydroxyapatite (b, c, and d). Red arrows indicate extrafibrillar minerals.

activate the MMPs.[44] The α-helix of collagen protein consists of three polypeptide chains; each with a repeating triplet sequence (-Gly-X-Y-)$_3$. The most common sequence is (-Gly-Pro-Hyp). Hyp is uncommon in other proteins, so can be used as a characteristic marker in collagen protein.[45] ELISA was used to detect the concentration of Hyp, which in turn indicated the amount of degraded collagen fibrils.

As shown in Figure 10, the data for the control group indicated the amount of collagen degradation under natural conditions. The high level of the cumulative Hyp concentration reflected the high rate of collagen degradation in the absence of intervention. Few undegraded collagen fibrils remained in the dentin powder after 24 h. The Hyp concentration decreased as the solution was progressively diluted. The data for the N-ACP group were the same as that of the control group since N-ACP released no chlorhexidine ($P > 0.05$).

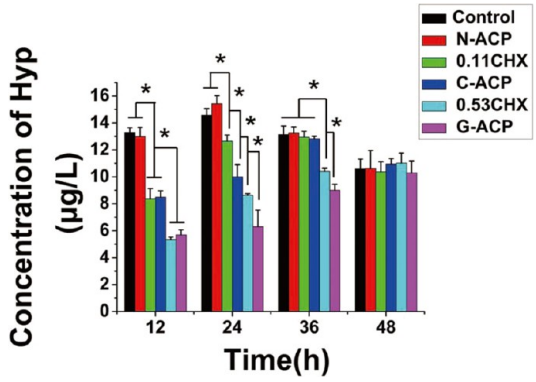

Figure 10. Cumulative concentration of Hyp, as a result of collagen degradation. * indicates a significant difference ($P < 0.05$) between groups.

The initial concentrations of chlorhexidine in the 0.11CHX and 0.53CHX groups corresponded to the chlorhexidine loadings in C-ACP and G-ACP, respectively. The four groups all inhibited collagen degradation over a 12 h duration ($P < 0.05$). The 0.53CHX and G-ACP groups contained more chlorhexidine, so the effects of inhibition were more pronounced ($P < 0.05$). After 24 h, the samples had been sufficiently diluted to be ineffective. The concentrations of chlorhexidine in the 0.11CHX and 0.53CHX groups decreased proportionally and finally failed to inhibit collagen degradation. However, C-ACP and G-ACP were able to continuously inhibit collagen degradation.

This result indicated that the effects of C-ACP and G-ACP lasted longer than those of pure chlorhexidine, at a similar concentration ($P < 0.05$). This result was attributed to the sustained release from C-ACP and G-ACP, which supplemented the chlorhexidine dose after each sampling dilution. In addition, the dentine powder was mixed well with the C-ACP and G-ACP nanoparticles in a stable manner. The chlorhex-

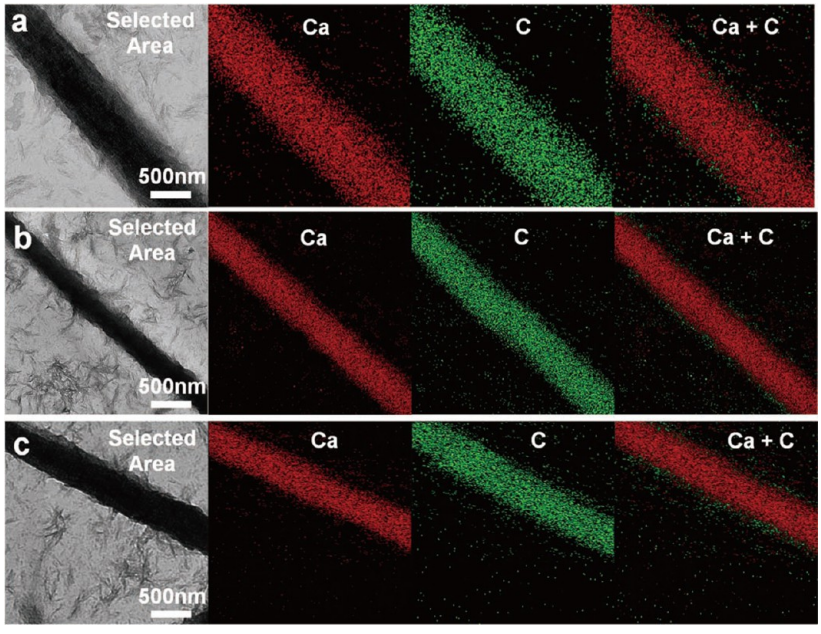

Figure 9. TEM images and elemental maps of Ca and C in (a) N-ACP, (b) C-ACP, and (c) G-ACP nanoparticles.

DOI: 10.1021/acsami.6b14956
ACS Appl. Mater. Interfaces 2017, 9, 12949−12958

idine could easily contact the dentine collagen without diffusing into the surrounding solution. Thus, C-ACP and G-ACP were able to maintain a higher local chlorhexidine concentration.

Chlorhexidine reportedly has a broad-spectrum MMP-inhibitory effect, even at very low concentrations of 0.1−2 wt %.[5,19,46] The current results suggested that 0.11 wt % was an effective chlorhexidine concentration, so were consistent with previous studies.[5,19] The sustained release ensured that the chlorhexidine concentration was maintained above the effective threshold. Collagen degradation was only observed 12 h after etching and slower than the control group. When the mineralization of collagen fibrils had not been completed, chlorhexidine prevented collagen from degrading and maintained the template for remineralization.

These findings suggest that the two types of chlorhexidine-loaded ACP nanoparticles carried out their respective roles well. Since this experimental situation was extreme, far less water and reacting area would be in the real bonding interface. The inhibition effect may last longer in real situation. Further studies will focus on the combined effects in mineral-depleted, resin-sparse, water-rich regions along the real bonding interface.

4. CONCLUSION

Chlorhexidine-loaded ACP nanoparticles were synthesized by a template technique, and sustained drug release properties were achieved. The resulting nanoparticles were successfully characterized by scanning electron microscopy, transmission electron microscopy, energy dispersive X-ray spectroscopy, BET surface area, pore size analysis, dynamic light scattering, and X-ray diffraction analysis. The C-ACP and G-ACP nanoparticles were able to inhibit the degradation of dentine collagen by the sustained release of chlorhexidine and induce the mineralization of collagen fibrils. It may have advantages in resin dentine bonding procedure, yet requires further study.

AUTHOR INFORMATION

Corresponding Author

*22 Zhongguancun Avenue South, Haidian District, Beijing 100081, P. R. China. E-mail: wangxiaoyan@pkuss.bjmu.edu.cn.

ORCID

Xue Cai: 0000-0002-0768-4076

Author Contributions

‖X.C. and B.H. contributed equally to this work.

Notes

The authors declare no competing financial interest.

ACKNOWLEDGMENTS

We acknowledge financial support from the National Natural Science Foundation of China (No. 81400562), Beijing Municipal Science & Technology Commission Project (No. Z141100000514016), and Peking University School of Stomatology (No. PKUSS20150111).

REFERENCES

(1) Liu, Y.; Mai, S.; Li, N.; Yiu, C. K.; Mao, J.; Pashley, D. H.; Tay, F. R. Differences Between Top-Down and Bottom-Up Approaches in Mineralizing Thick, Partially Demineralized Collagen Scaffolds. *Acta Biomater.* **2011**, *7*, 1742−1751.

(2) Pasteris, J. D.; Wopenka, B.; Valsami-Jones, E. Bone and Tooth Mineralization: Why Apatite? *Elements* **2008**, *4*, 97−104.

(3) Wang, J. M.; Chen, Y.; Li, L.; Sun, J.; Gu, X. H.; Xu, X.; Pan, H.; Tang, R. Remineralization of Dentin Collagen by Meta-Stabilized Amorphous Calcium Phosphate. *CrystEngComm* **2013**, *15*, 6151−6158.

(4) Fu, Y.; Liu, S.; Cui, S. J.; Kou, X. X.; Wang, X. D.; Liu, X. M.; Sun, Y.; Wang, G. N.; Liu, Y.; Zhou, Y. H. Surface Chemistry of Nanoscale Mineralized Collagen Regulates Periodontal Ligament Stem Cell Fate. *ACS Appl. Mater. Interfaces* **2016**, *8*, 15958−15966.

(5) Breschi, L.; Mazzoni, A.; Nato, F.; Carrilho, M.; Visintini, E.; Tjäderhane, L.; Ruggeri, A.; Tay, F. R.; Dorigo, E. D. S.; Pashley, D. H. Chlorhexidine Stabilizes the Adhesive Interface: A 2-Year in Vitro Study. *Dent. Mater.* **2010**, *26*, 320−325.

(6) Pashley, D. H.; Agee, K. A.; Wataha, J. C.; Rueggeberg, F.; Ceballos, L.; Itou, K.; Yoshiyama, M.; Carvalho, R. M.; Tay, F. R. Viscoelastic Properties of Demineralized Dentin Matrix. *Dent. Mater.* **2003**, *19*, 700−706.

(7) Fung, D. T.; Wang, V. M.; Laudier, D. M.; Shine, J. H.; Basta-Pljakic, J.; Jepsen, K. J.; Schaffler, M. B.; Flatow, E. L. Subrupture Tendon Fatigue Damage. *J. Orthop. Res.* **2009**, *27*, 264−273.

(8) Mazzoni, A.; Pashley, D. H.; Nishitani, Y.; Breschi, L.; Mannello, F.; Tjaderhane, L.; Toledano, M.; Pashley, E. L.; Tay, F. R. Reactivation of Inactivated Endogenous Proteolytic Activities in Phosphoric Acid-Etched Dentine by Etch-And-Rinse Adhesives. *Biomaterials* **2006**, *27*, 4470−4476.

(9) Niu, L.; Zhang, W.; Pashley, D. H.; Breschi, L.; Mao, J.; Chen, J.; Tay, F. R. Biomimetic Remineralization of Dentin. *Dent. Mater.* **2014**, *30*, 77−96.

(10) Sauro, S.; Watson, T. F.; Mannocci, F.; Miyake, K.; Huffman, B. P.; Tay, F. R.; Pashley, D. H. Two-Photon Laser Confocal Microscopy of Micropermeability of Resin-Dentin Bonds Made with Water Or Ethanol Wet Bonding. *J. Biomed. Mater. Res., Part B* **2009**, *90*, 327−337.

(11) Tay, F. R.; Pashley, D. H. Water Treeing–A Potential Mechanism for Degradation of Dentin Adhesives. *Am. J. Dent.* **2003**, *16*, 6−12.

(12) Reis, A. F.; Giannini, M.; Pereira, P. N. R. Long-Term TEM Analysis of the Nanoleakage Patterns in Resin−Dentin Interfaces Produced by Different Bonding Strategies. *Dent. Mater.* **2007**, *23*, 1164−1172.

(13) Liu, Y.; Tjaderhane, L.; Breschi, L.; Mazzoni, A.; Li, N.; Mao, J.; Pashley, D. H.; Tay, F. R. Limitations in Bonding to Dentin and Experimental Strategies to Prevent Bond Degradation. *J. Dent. Res.* **2011**, *90*, 953−968.

(14) Jokstad, A.; Bayne, S.; Blunck, U.; Tyas, M.; Wilson, N. Quality of Dental Restorations. FDI Commission Project 2−95. *Int. Dent. J.* **2001**, *51*, 117−158.

(15) Liu, Y.; Kim, Y.; Dai, L.; Li, N.; Khan, S. O.; Pashley, D. H.; Tay, F. R. Hierarchical and Non-Hierarchical Mineralisation of Collagen. *Biomaterials* **2011**, *32*, 1291−1300.

(16) Liu, Y.; Li, N.; Qi, Y.; Niu, L.; Elshafiy, S.; Mao, J.; Breschi, L.; Pashley, D. H.; Tay, F. R. The Use of Sodium Trimetaphosphate as a Biomimetic Analog of Matrix Phosphoproteins for Remineralization of Artificial Caries-Like Dentin. *Dent. Mater.* **2011**, *27*, 465−477.

(17) Breschi, L.; Mazzoni, A.; Ruggeri, A.; Cadenaro, M.; Di Lenarda, R.; De Stefano, D. E. Dental Adhesion Review: Aging and Stability of the Bonded Interface. *Dent. Mater.* **2008**, *24*, 90−101.

(18) Zhang, S. C.; Kern, M. The Role of Host-derived Dentinal Matrix Metalloproteinases in Reducing Dentin Bonding of Resin Adhesives. *Int. J. Oral Sci.* **2009**, *1*, 163−176.

(19) Zhou, J.; Tan, J.; Chen, L.; Li, D.; Tan, Y. The Incorporation of Chlorhexidine in a Two-Step Self-Etching Adhesive Preserves Dentin Bond in Vitro. *J. Dent.* **2009**, *37*, 807−812.

(20) Carrilho, M. R.; Geraldeli, S.; Tay, F.; de Goes, M. F.; Carvalho, R. M.; Tjaderhane, L.; Reis, A. F.; Hebling, J.; Mazzoni, A.; Breschi, L.; Pashley, D. In Vivo Preservation of the Hybrid Layer by Chlorhexidine. *J. Dent. Res.* **2007**, *86*, 529−533.

(21) Breschi, L.; Cammelli, F.; Visintini, E.; Mazzoni, A.; Vita, F.; Carrilho, M.; Cadenaro, M.; Foulger, S.; Mazzoti, G.; Tay, F. R.; Di Lenarda, R.; Pashley, D. Influence of Chlorhexidine Concentration On the Durability of Etch-And-Rinse Dentin Bonds: A 12-Month in Vitro Study. *J. Adhes. Dent.* **2009**, *11*, 191−198.

DOI: 10.1021/acsami.6b14956
ACS Appl. Mater. Interfaces 2017, 9, 12949−12958

(22) Sadek, F. T.; Braga, R. R.; Muench, A.; Liu, Y.; Pashley, D. H.; Tay, F. R. Ethanol Wet-Bonding Challenges Current Anti-Degradation Strategy. *J. Dent. Res.* **2010**, *89*, 1499−1504.
(23) Yue, I. C.; Poff, J.; Cortes, M. E.; Sinisterra, R. D.; Faris, C. B.; Hildgen, P.; Langer, R.; Shastri, V. P. A Novel Polymeric Chlorhexidine Delivery Device for the Treatment of Periodontal Disease. *Biomaterials* **2004**, *25*, 3743−3750.
(24) Mundargi, R. C.; Srirangarajan, S.; Agnihotri, S. A.; Patil, S. A.; Ravindra, S.; Setty, S. B.; Aminabhavi, T. M. Development and Evaluation of Novel Biodegradable Microspheres Based On Poly(D,L-Lactide-Co-Glycolide) and Poly(Epsilon-Caprolactone) for Controlled Delivery of Doxycycline in the Treatment of Human Periodontal Pocket: In Vitro and in Vivo Studies. *J. Controlled Release* **2007**, *119*, 59−68.
(25) Li, Y.; Li, D.; Weng, W. Amorphous Calcium Phosphates and its Biomedical Application. *J. Inorg. Mater.* **2007**, *22*, 775−782.
(26) Mahamid, J.; Sharir, A.; Addadi, L.; Weiner, S. Amorphous Calcium Phosphate is a Major Component of the Forming Fin Bones of Zebrafish: Indications for an Amorphous Precursor Phase. *Proc. Natl. Acad. Sci. U. S. A.* **2008**, *105*, 12748−12753.
(27) Rho, J.; Kuhn-Spearing, L.; Zioupos, P. Mechanical Properties and the Hierarchical Structure of Bone. *Med. Eng. Phys.* **1998**, *20*, 92−102.
(28) Cheng, X.; Gower, L. B. Molding Mineral within Microporous Hydrogels by a Polymer-Induced Liquid-Precursor (PILP) Process. *Biotechnol. Prog.* **2006**, *22*, 141−149.
(29) Niu, L. N.; Jee, S. E.; Jiao, K.; Tonggu, L.; Li, M.; Wang, L.; Yang, Y. D.; Bian, J. H.; Breschi, L.; Jang, S. S.; Chen, J. H.; Pashley, D. H.; Tay, F. R. Collagen Intrafibrillar Mineralization as a Result of the Balance Between Osmotic Equilibrium and Electroneutrality. *Nat. Mater.* **2016**, *16*, 370.
(30) Combes, C.; Rey, C. Amorphous Calcium Phosphates: Synthesis, Properties and Uses in Biomaterials. *Acta Biomater.* **2010**, *6*, 3362−3378.
(31) Seeherman, H. J.; Azari, K.; Bidic, S.; Rogers, L.; Li, X. J.; Hollinger, J. O.; Wozney, J. M. rhBMP-2 Delivered in a Calcium Phosphate Cement Accelerates Bridging of Critical-Sized Defects in Rabbit Radii. *J. Bone Jt. Surg., Am. Vol.* **2006**, *88*, 1553−1565.
(32) Rodrigues, M. C.; Natale, L. C.; Arana-Chaves, V. E.; Braga, R. R. Calcium and Phosphate Release From Resin-Based Materials Containing Different Calcium Orthophosphate Nanoparticles. *J. Biomed. Mater. Res., Part B* **2015**, *103*, 1670−1678.
(33) Xu, H. H. K.; Moreau, J. L.; Sun, L.; Chow, L. C. Nanocomposite Containing Amorphous Calcium Phosphate Nanoparticles for Caries Inhibition. *Dent. Mater.* **2011**, *27*, 762−769.
(34) He, W.; Tang, R.; Xu, X. Synthesis of Hollow Amorphous Calcium Phosphate for Drug Delivery. *Chin. J. Inorg. Chem.* **2011**, *27*, 1233−1238.
(35) Tay, F. R.; Pashley, D. H.; Loushine, R. J.; Weller, R. N.; Monticelli, F.; Osorio, R. Self-Etching Adhesives Increase Collagenolytic Activity in Radicular Dentin. *J. Endod.* **2006**, *32*, 862−868.
(36) Liu, T.; Guo, R. Preparation of a Highly Stable Niosome and its Hydrotrope-Solubilization Action to Drugs. *Langmuir* **2005**, *21*, 11034−11039.
(37) Bayindir, Z. S.; Yuksel, N. Characterization of Niosomes Prepared with Various Nonionic Surfactants for Paclitaxel Oral Delivery. *J. Pharm. Sci.* **2010**, *99*, 2049−2060.
(38) Ding, G. J.; Zhu, Y. J.; Qi, C.; Lu, B. Q.; Wu, J.; Chen, F. Porous Microspheres of Amorphous Calcium Phosphate: Block Copolymer Templated Microwave-assisted Hydrothermal Synthesis and Application in Drug Delivery. *J. Colloid Interface Sci.* **2015**, *443*, 72−79.
(39) Aizenberg, J.; Lambert, G.; Weiner, S.; Addadi, L. Factors Involved in the Formation of Amorphous and Crystalline Calcium Carbonate: a Study of an Ascidian Skeleton. *J. Am. Chem. Soc.* **2002**, *124*, 32−39.
(40) Liou, S. C.; Chen, S. Y.; Liu, D. M. Manipulation of Nanoneedle and Nanosphere Apatite/Poly(Acrylic Acid) Nanocomposites. *J. Biomed. Mater. Res., Part B* **2005**, *73*, 117−122.
(41) Costa, P.; Lobo, J. M. S. Modeling and Comparison of Dissolution Profiles. *Eur. J. Pharm. Sci.* **2001**, *13*, 123−133.
(42) Bowen, W. H. The Stephan Curve Revisited. *Odontology* **2013**, *101*, 2−8.
(43) Gajjeraman, S.; Narayanan, K.; Hao, J.; Qin, C.; George, A. Matrix Macromolecules in Hard Tissues Control the Nucleation and Hierarchical Assembly of Hydroxyapatite. *J. Biol. Chem.* **2007**, *282*, 1193−1204.
(44) Pashley, D. H.; Tay, F. R.; Yiu, C.; Hashimoto, M.; Breschi, L.; Carvalho, R. M.; Ito, S. Collagen degradation by host-derived enzymes during aging. *J. Dent. Res.* **2004**, *83*, 216−221.
(45) Bhattacharjee, A.; Bansal, M. Collagen Structure: The Madras Triple Helix and the Current Scenario. *IUBMB Life* **2005**, *57*, 161−172.
(46) Gendron, R.; Grenier, D.; Sorsa, T.; Mayrand, D. Inhibition of the Activities of Matrix Metalloproteinases 2, 8, and 9 by Chlorhexidine. *Clin. Diagn. Lab. Immunol.* **1999**, *6*, 437−439.

DOI: 10.1021/acsami.6b14956
ACS Appl. Mater. Interfaces 2017, 9, 12949−12958